Cell Reports, Volume *43*

Supplemental information

LXR/CD38 activation drives cholesterol-induced macrophage senescence and neurodegeneration via NAD^+ depletion

Ryo Terao, Tae Jun Lee, Jason Colasanti, Charles W. Pfeifer, Joseph B. Lin, Andrea Santeford, Keitaro Hase, Shinobu Yamaguchi, Daniel Du, Brian S. Sohn, Yo Sasaki, Mitsukuni Yoshida, and Rajendra S. Apte

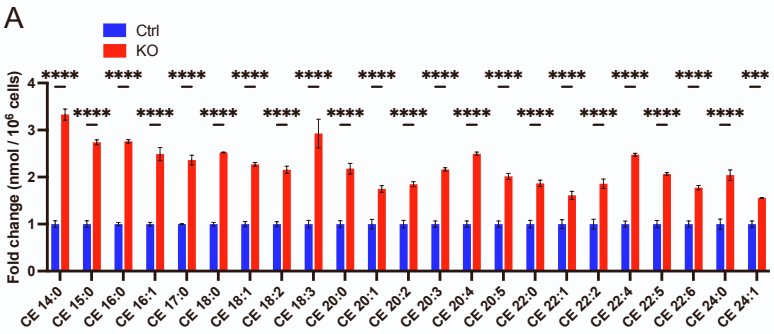
A
Ctrl
KO
Fold change (nmol / 10^6 cells)
CE 14:0
CE 15:0
CE 16:0
CE 16:1
CE 17:0
CE 18:0
CE 18:1
CE 18:2
CE 18:3
CE 20:0
CE 20:1
CE 20:2
CE 20:3
CE 20:4
CE 20:5
CE 22:0
CE 22:1
CE 22:2
CE 22:4
CE 22:5
CE 22:6
CE 24:0
CE 24:1

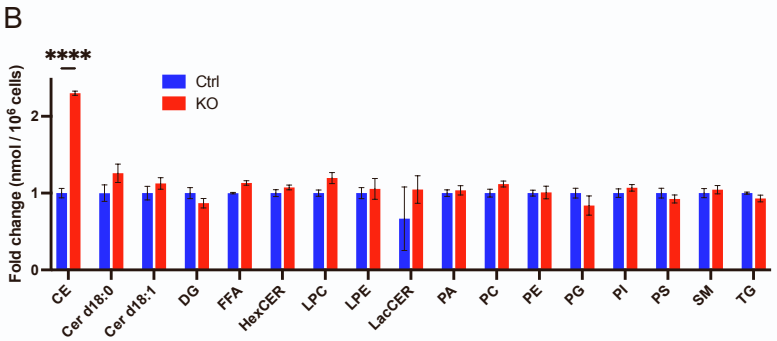
B
Ctrl
KO
Fold change (nmol / 10^6 cells)
CE
Cer d18:0
Cer d18:1
DG
FFA
HexCER
LPC
LPE
LacCER
PA
PC
PE
PG
PI
PS
SM
TG

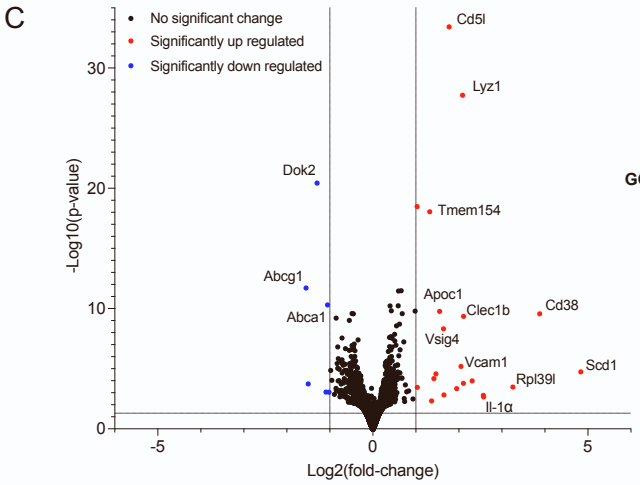
C
No significant change
Significantly up regulated
Significantly down regulated
-Log10(p-value)
Log2(fold-change)
Cd5l
Lyz1
Dok2
Tmem154
Abcg1
Abca1
Apoc1
Clec1b
Cd38
Vsig4
Vcam1
Rpl39l
Scd1
Il-1α

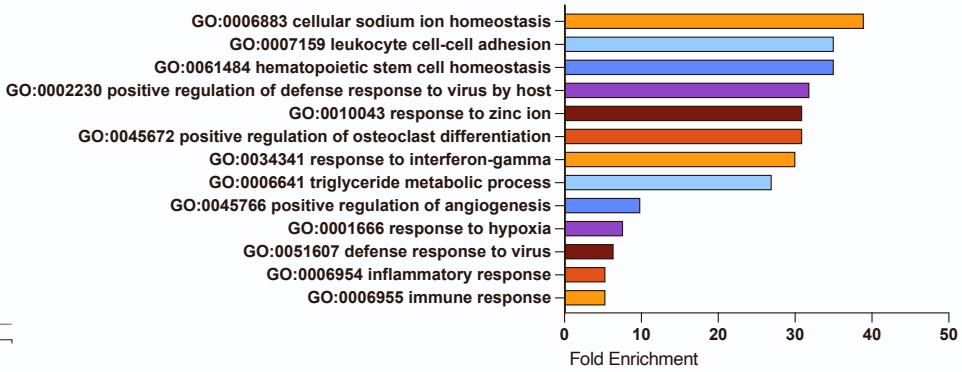
D
GO:0006883 cellular sodium ion homeostasis
GO:0007159 leukocyte cell-cell adhesion
GO:0061484 hematopoietic stem cell homeostasis
GO:0002230 positive regulation of defense response to virus by host
GO:0010043 response to zinc ion
GO:0045672 positive regulation of osteoclast differentiation
GO:0034341 response to interferon-gamma
GO:0006641 triglyceride metabolic process
GO:0045766 positive regulation of angiogenesis
GO:0001666 response to hypoxia
GO:0051607 defense response to virus
GO:0006954 inflammatory response
GO:0006955 immune response
Fold Enrichment

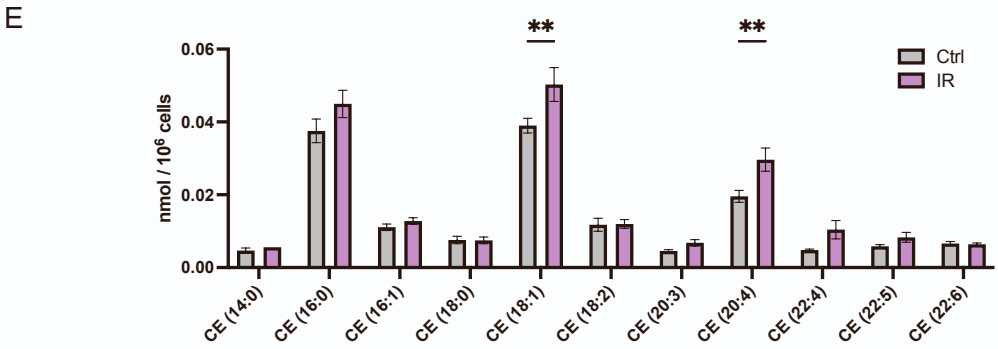
E
Ctrl
IR
nmol / 10^6 cells
CE (14:0)
CE (16:0)
CE (16:1)
CE (18:0)
CE (18:1)
CE (18:2)
CE (20:3)
CE (20:4)
CE (22:4)
CE (22:5)
CE (22:6)

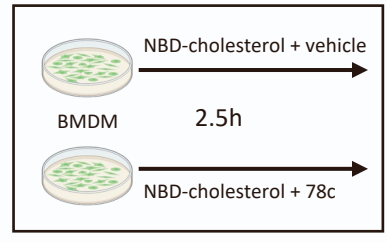
F
NBD-cholesterol + vehicle
BMDM
2.5h
NBD-cholesterol + 78c

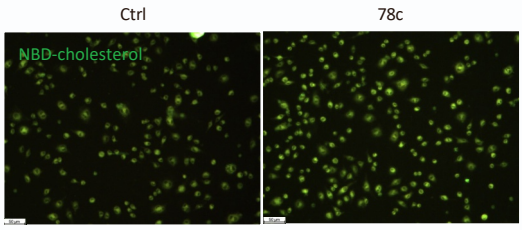
G
Ctrl
78c
NBD-cholesterol

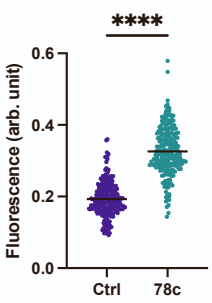
H
Fluorescence (arb. unit)
Ctrl
78c

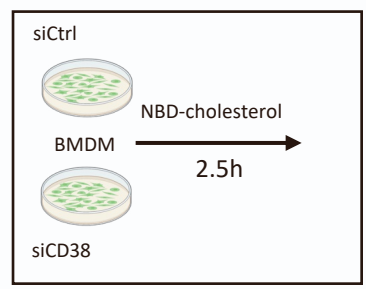
I
siCtrl
NBD-cholesterol
BMDM
2.5h
siCD38

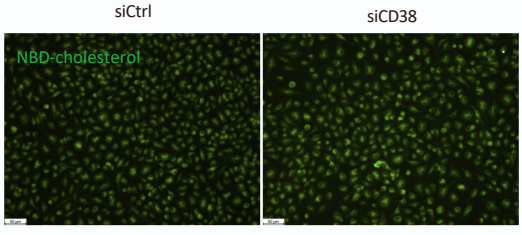
J
siCtrl
siCD38
NBD-cholesterol

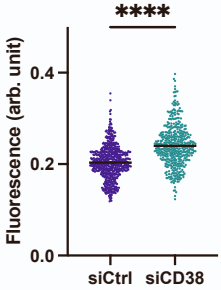
K
Fluorescence (arb. unit)
siCtrl
siCD38

Figure S1. Lipid profiles and bulk RNA sequence of macrophages with *Abca1* and *Abcg1* deficiency and the effect of CD38 inhibition on cholesterol accumulation in macrophages, related to Figure 1

(A) Intracellular cholesterol ester (CE) species in *Abca1/g1*$^{-m/-m}$ (KO) and *Abca1/g1*$^{f/f}$ (Ctrl) BMDMs. (B) Quantitative profiles of lipid classes in KO and Ctrl BMDMs. (C) The volcano plot of genes generated using a $\log_2$ -fold change and corrected *p* values between KO and Ctrl BMDMs. Cutoff of -$\log_{10}$(p. value) and $\log_2$(fold-change) are set to 1.3 and ±1.0, respectively. (D) Gene set enrichment analysis of *Abca1/g1*$^{-m/-m}$ BMDMs compared with *Abca1/g1*$^{f/f}$ BMDMs. (E) Intracellular CE species in BMDMs treated with irradiation (IR). (F) Experimental design of NBD-cholesterol flux assay using 78c (G) Representative images of BMDMs treated with NBD-cholesterol under the presence of 78c or vehicle (DMSO). (H) The quantification of fluorescence intensity of each cell. (I) Experimental design of NBD-cholesterol flux assay using siRNA knockdown of *CD38* (siCD38). (J) Representative images of BMDMs transfected with siCrtl or siCD38 and treated with NBD-cholesterol. (K) The quantification of fluorescence intensity of each cell. Cer, ceramide; DG, diglycerides; FFA, free fatty acids; HexCER, Hexosylceramides; LPC, lysophosphatidylcholines; LPE, lysophosphatidylethanolamine; LacCER, lactosylceramide; PA, phosphatidic acid; PC, phosphatidylcholines; PE, phosphatidylethanolamine; PG, phosphatidylglycerol; PI, phosphatidylinositol; PS, phosphatidylserine; SM, sphingomyelin; TG, triglyceride. ***p < 0.001; ****p < 0.0001, two-way ANOVA followed by Bonferroni correction for comparison. Data are represented as mean ± SEM. The length of scale bar is indicated in each image.

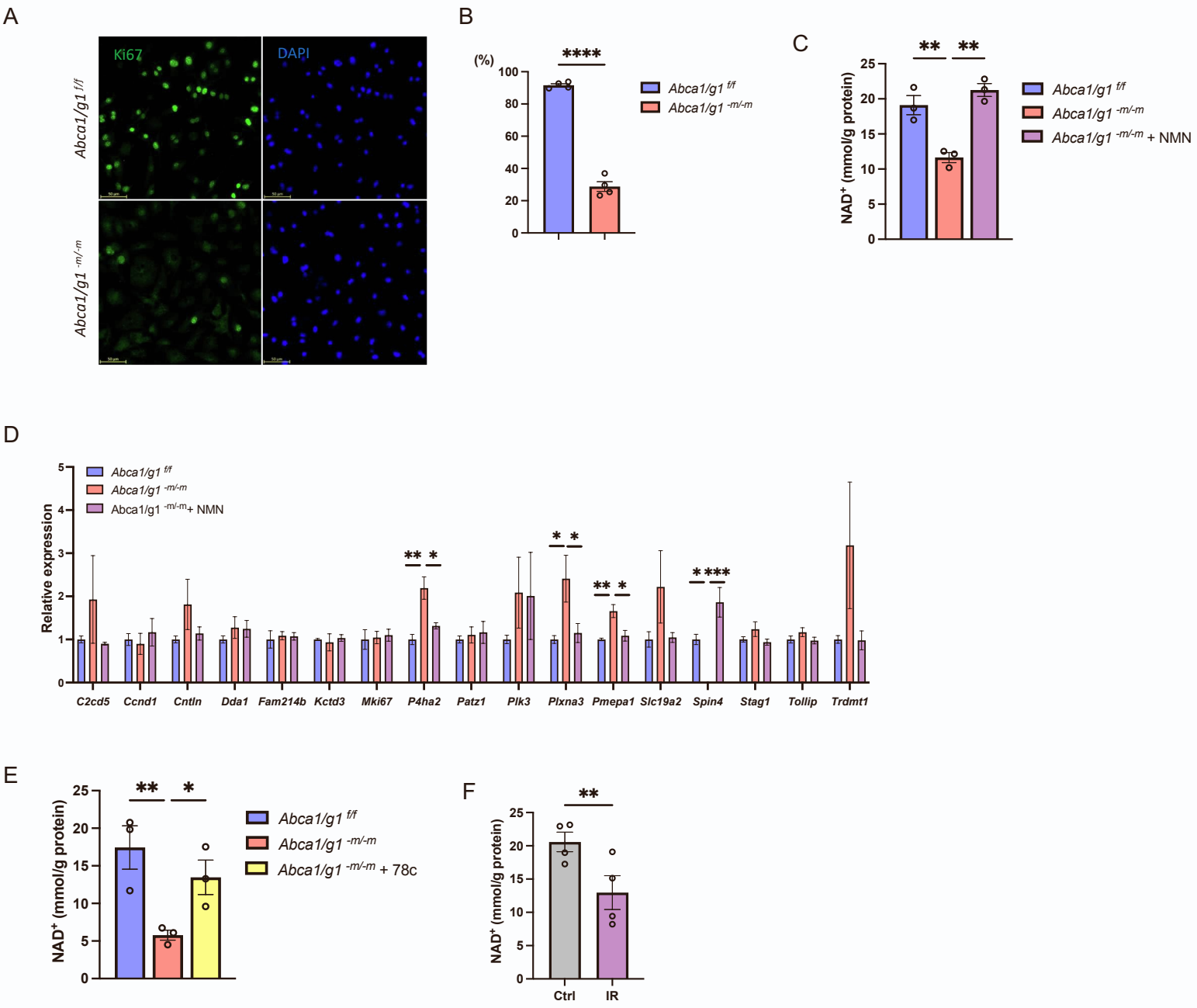

Figure S2. Senescence profiles of macrophages with Abca1 and Abcg1 deficiency, related to Figure 2

(A) Immunofluorescence of Ki76 of BMDMs isolated from *Abca1/g1*$^{f/f}$ and *Abca1/g1*$^{-m/-m}$ mice. (B) The quantification of Ki67-positive cells. (C) NAD^+ concentration of *Abca1/g1*$^{-m/-m}$ BMDMs treated with NMN. (D) Senescence panel assay to evaluate senescence markers in *Abca1/g1*$^{f/f}$, *Abca1/g1*$^{-m/-m}$, and *Abca1/g1*$^{-m/-m}$ BMDMs treated with NMN. (E) NAD^+ concentration of *Abca1/g1*$^{-m/-m}$ BMDMs treated with the CD38 inhibitor. (F) NAD^+ concentration of BMDMs treated with irradiation (IR). *p < 0.05; **p < 0.01; ***p < 0.001; ****p < 0.0001, t-test for comparison between 2 groups, one-way ANOVA followed by Bonferroni correction for comparison. Data are represented as mean ± SEM. The length of scale bar is indicated in each image.

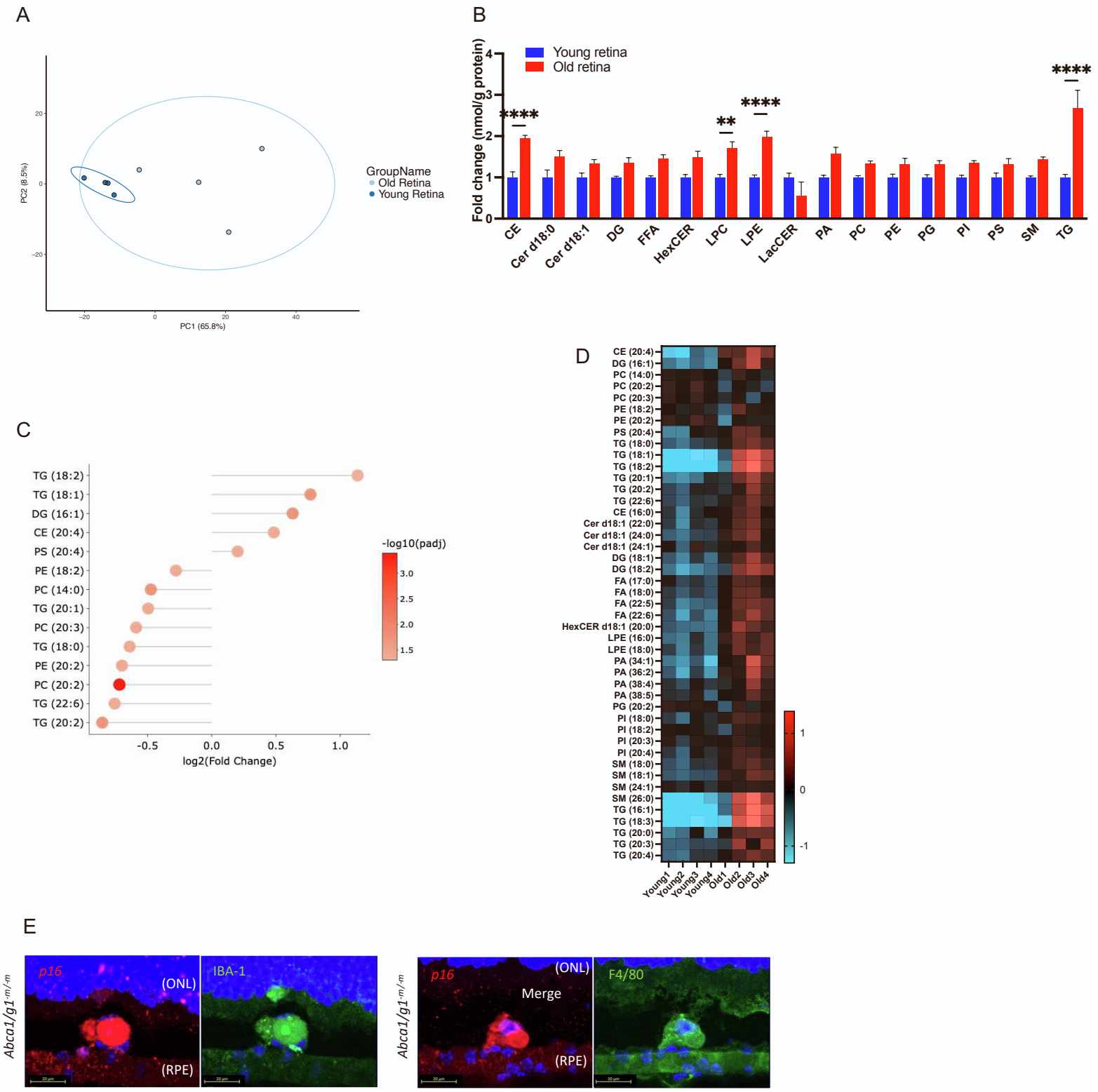

Figure S3. Lipid profiles of retina isolated from young and old mice, related to Figure 3

(A) Principal component analyses (PCA) analysis of the lipidmics data in young (2 months old) and old (27 months old) retina quantified by LC/MS. (B) Quantitative profiles of lipid classes in young and old retina. (C) The lollipop chart of lipid species with significance analysed by LipidSig. (D) The heatmap increased lipids in lipidomics measurement. (E) Co-staining images of ISH (*p16*) and immunofluorescence (F4/80 and IBA-1) in retinal sections. ONL, outer nuclear layer; RPE, retinal pigment epithelium. Cer, ceramide; DG, diglycerides; FFA, free fatty acids; HexCER, Hexosylceramides; LPC, lysophosphatidylcholines; LPE, lysophosphatidylethanolamine; LacCER, lactosylceramide; PA, phosphatidic acid; PC, phosphatidylcholines; PE, phosphatidylethanolamine; PG, phosphatidylglycerol; PI, phosphatidylinositol; PS, phosphatidylserine; SM, sphingomyelin; TG, triglyceride. **p < 0.01; ****p < 0.0001, two-way ANOVA followed by Bonferroni correction for comparison. Data are represented as mean ± SEM. The length of scale bar is indicated in each image.

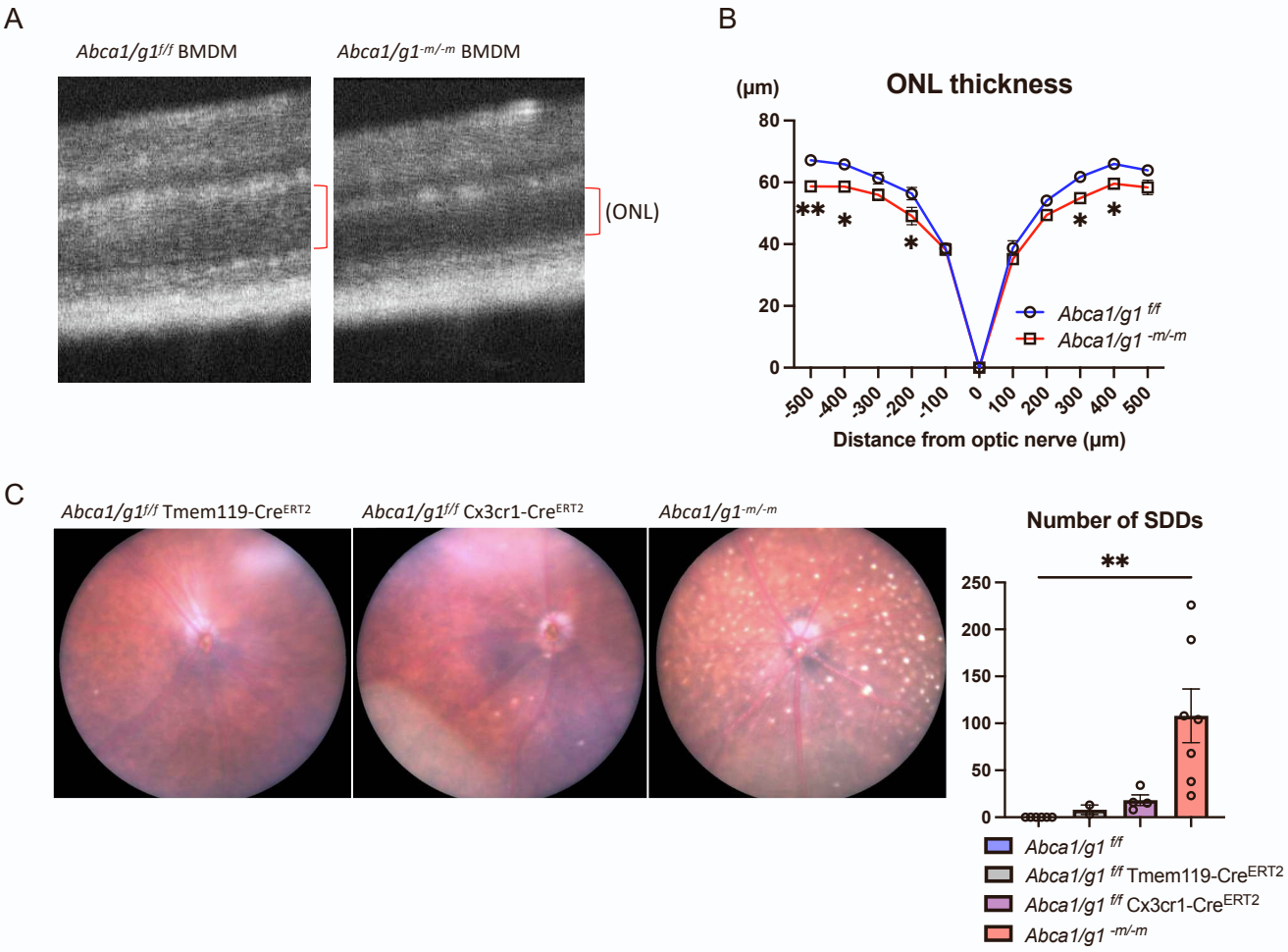

Figure S4. Subretinal senescent macrophages induce photoreceptor degeneration, related to Figure 4

(A) Representative optical coherence tomography images of wild-type mice treated with subretial injection of BMDMs isolated from *Abca1/g1*$^{f/f}$ and *Abca1/g1*$^{-m/-m}$ mice. Brackets indicate outer nuclear layer (ONL), which contains photoreceptor nuclei. (B) Quantification of ONL thickness in retina treated with subretinal BMDM injection. ONL thickness was measured at points every 100μm from optic nerve. (C) Representative fundus images of *Abca1/g1*$^{f/f}$ Tmem119-Cre^{ERT2}, *Abca1/g1*$^{f/f}$ Tmem119-Cre^{ERT2}, and *Abca1/g1*$^{-m/-m}$ mice. Images of mice expressing Cre^{ERT2} were taken 3 months after tamoxifen-infused chow feeding for 3 weeks. *p < 0.05; **p < 0.01; ***p < 0.001; ****p < 0.0001, two-way ANOVA followed by Bonferroni correction for comparison. Data are represented as mean ± SEM.

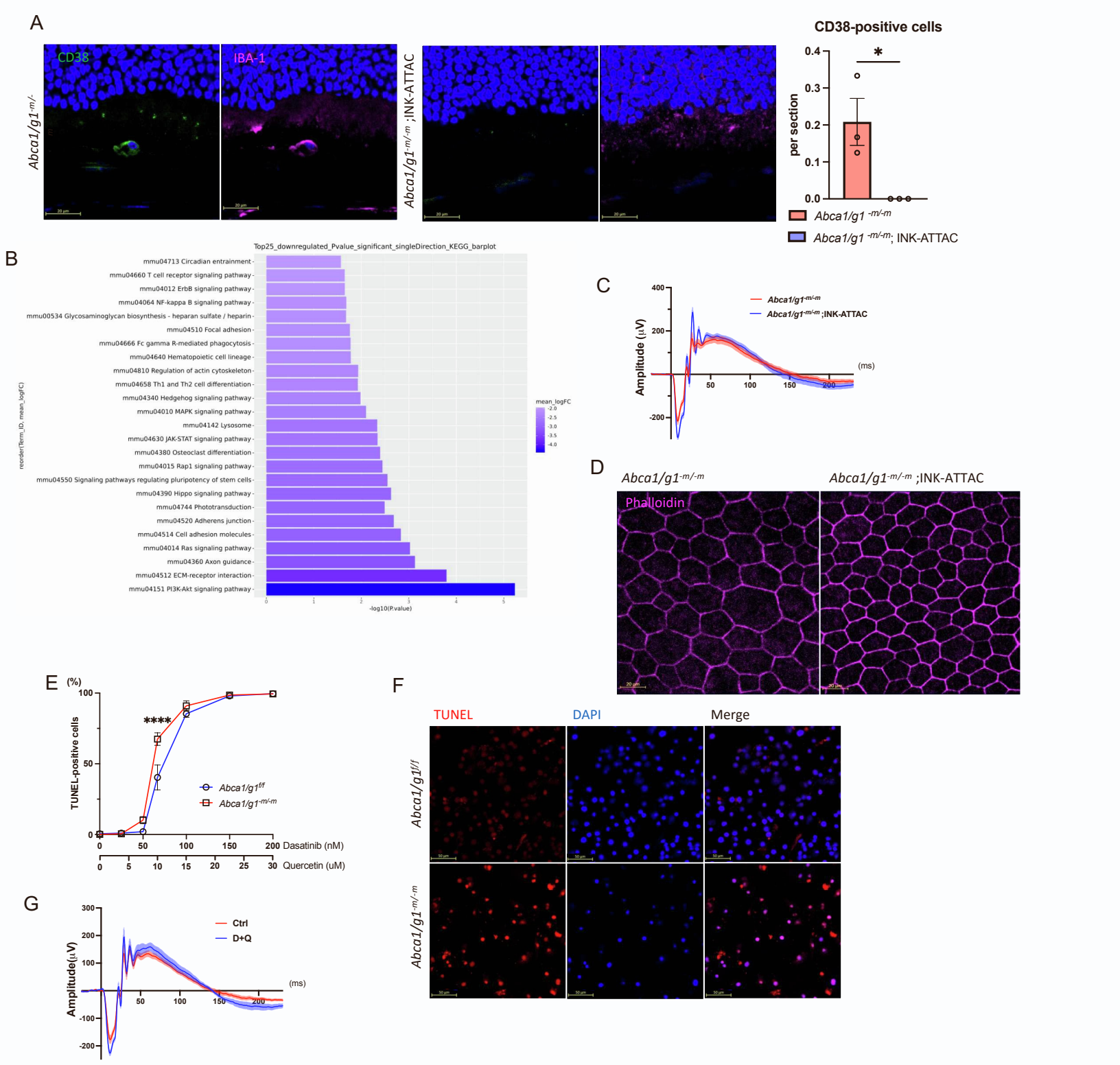

Figure S5. Effects of genetic and pharmacological senolysis on cellular signaling pathway in RPE/choroid complex and retinal function, related to Figure 5

(A) Immunofluorescence of CD38 and IBA-1 in retinal sections of *Abca1/g1*$^{-m/-m}$ and *Abca1/g1*$^{-m/-m}$; INK-ATTAC and the quantification of CD38-positive cells. (B) KEGG pathway analysis of genes comparing RPE/choroid complex samples isolated from *Abca1/g1*$^{-m/-m}$ and *Abca1/g1*$^{-m/-m}$; INK-ATTAC. (C) ERG wave of *Abca1/g1*$^{-m/-m}$ and *Abca1/g1*$^{-m/-m}$;INK-ATTAC. Each waveform indicates the mean ± SEM.. (D) Representative immunofluorescence images of RPE-flatmount isolated from *Abca1/g1*$^{-m/-m}$ and *Abca1/g1*$^{-m/-m}$;INK-ATTAC stained for phalloidin. Note the smaller number of RPE cells indicating cell loss in *Abca1/g1*$^{-m/-m}$. (E) The proportion of TUNEL-positive cells in *Abca1/g1*$^{f/f}$ and *Abca1/g1*$^{-m/-m}$ BMDMs treated with dasatinib and quercetin *in vitro*. (F) Representative TUNEL staining of *Abca1/g1*$^{f/f}$ and *Abca1/g1*$^{-m/-m}$ BMDMs treated with dasatinib (66.7nM) and quercetin (10uM). (G) ERG wave of *Abca1/g1*$^{-m/-m}$ treated with D+Q or vehicle (Ctrl). Each waveform indicates the mean ± SEM. *p < 0.05; ****p < 0.0001, t-test for comparison between 2 groups, two-way ANOVA followed by Bonferroni correction for comparison with multiple time points. Data are represented as mean ± SEM. The length of scale bar is indicated in each image.

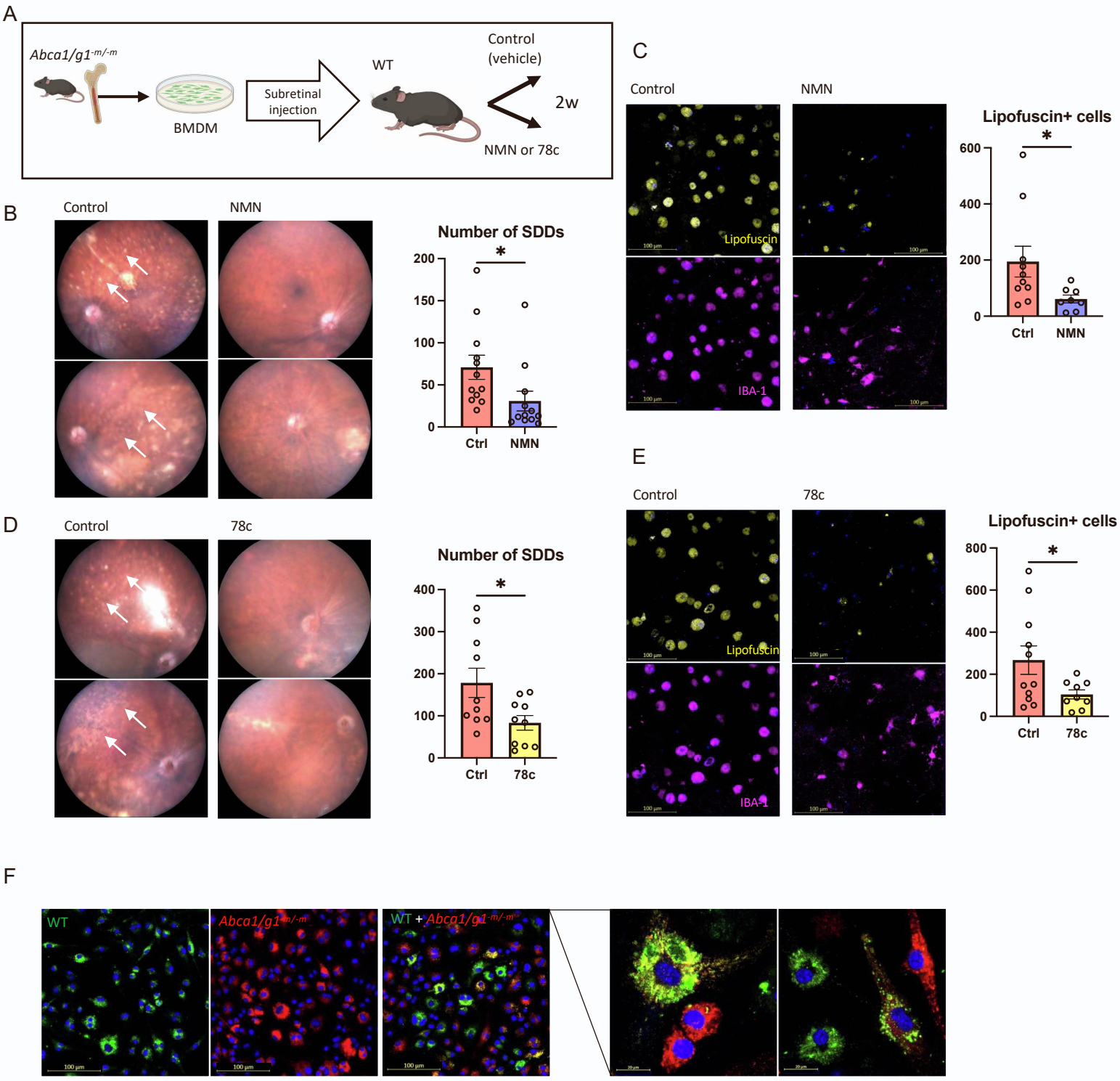

Figure S6. NAD+ augmentation promotes the clearance of subretinal senescent macrophages and drusenoid deposits, related to Figure 6.

(A) Experimental design for SDD induction by subretinal injection of *Abca1/g1*$^{-m/-m}$ BMDMs followed by treatment with NMN or CD38 inhibitor (78c). (B) Representative fundus images of eyes administered subretinal *Abca1/g1*$^{-m/-m}$ BMDMs injection followed by the treatment with NMN and the quantification of SDD. (C) Representative images of RPE-flatmount showing lipofuscin- and IBA-1-positive cells and the quantification of lipofuscin-positive cells. (D) Representative fundus images of eyes treated with subretinal *Abca1/g1*$^{-m/-m}$ BMDMs injection followed by the administration of 78c, and the quantification of SDD. (E) Representative images of RPE-flatmount showing lipofuscin- and IBA-1-positive cells and the quantification of lipofuscin-positive cells. (F) Co-incubation of *Abca1/g1*$^{-m/-m}$ (red) BMDMs with young healthy BMDMs (green). *$p < 0.05$, t-test for comparison between 2 groups. Data are represented as mean ± SEM. The length of scale bar is indicated in each image.

Supplementary Table 1. qPCR probes, related to STAR methods

Gene	Taqman gene reference
β-actin	Mm02619580_g1
Cdkn1a (*p21^{CIP1}*)	Mm04205640_g1
Cdkn2a (*p16^{Ink4a}*)	Mm00494449_m1
Cd38	Mm01220906_m1
Il-1β	Mm01336189_m1
Nampt	Mm01293559_m1
Nmnat1	Mm01257929_m1
Nmnat3	Mm00513791_m1
Tnf-α	Mm00443258_m1
Vcam1	Mm01320970_m1
Vegf-a	Mm01281449_m1